Biochimica et Biophysica Acta 1838 (2014) 1871–1880

Contents lists available at ScienceDirect

Biochimica et Biophysica Acta

journal homepage: www.elsevier.com/locate/bbamem

The effects of temperature, salinity, concentration and PEGylated lipid on the spontaneous nanostructures of bicellar mixtures

Ying Liu [a], Ming Li [b], Yongkun Yang [b], Yan Xia [a], Mu-Ping Nieh [a,b,c,*]

[a] Department of Chemical and Biomolecular Engineering, University of Connecticut, Storrs, CT 06269, USA
[b] Polymer Program, Institute of Materials Science, University of Connecticut, Storrs, CT 06269, USA
[c] Department of Biomedical Engineering, University of Connecticut, Storrs, CT 06269, USA

ARTICLE INFO

Article history:
Received 26 August 2013
Received in revised form 23 December 2013
Accepted 11 February 2014
Available online 21 February 2014

Keywords:
Bicelle
Unilamellar vesicle (ULV)
Structural transition
Thermodynamic stability
PEG effect
Salt effect
SANS

ABSTRACT

The self-assembling morphologies of low-concentration (mostly 1 and 10 mg/mL) bicellar mixtures composed of zwitterionic dipalmitoyl (di-C_{16}) phosphatidylcholine (DPPC), dihexanoyl (di-C_6) phosphatidylcholine (DHPC), and negatively charged dipalmitoyl (di-C_{16}) phosphatidylglycerol (DPPG) were investigated using small angle neutron scattering, dynamic light scattering and transmission electron microscopy. A polyethylene glycol conjugated (PEGylated) lipid, distearoyl phosphoethanolamine-[methoxy (polyethyleneglycol)-2000] (PEG2000-DSPE), was incorporated in the system at 5 mol% of the total lipid composition. The effects of several parameters on the spontaneous structures were studied, including temperature, lipid concentration, salinity, and PEG2000-DSPE. In general, nanodiscs (bicelles) were observed at low temperatures (below the melting temperature, T_M of DPPC) depending on the salinity of the solutions. Nanodisc-to-vesicle transition was found upon the elevation of temperature (above T_M) in the cases of low lipid concentration in the absence of PEG2000-DSPE or high salinity. Both addition of PEG2000-DSPE and high lipid concentration stabilize the nanodiscs, preventing the formation of multilamellar vesicles, while high salinity promotes vesiculation and the formation of aggregation. This study suggests that the stability of such nanodiscs is presumably controlled by the electrostatic interactions, the steric effect induced by PEG2000-DSPE, and the amount of DHPC located at the disc rim.

Published by Elsevier B.V.

1. Introduction

Phospholipids, being the major building blocks of biological membranes, are fundamentally important species that provide the environment for and interact with membrane-associated proteins to achieve specific functions (e.g., signaling, molecular translocation, enzymatic activity, adhesion) on the membrane. Many efforts have been made to understand the interaction between membrane proteins and phospholipids as well as their structures on the membranes. To probe the structure of membrane proteins in their native environment (i.e., bilayer), an emerging phospholipid mixture known as "bicelle", which is normally composed of long- and short-chain lipids, has been developed. This system is suitable for nuclear magnetic resonance (NMR) studies because of its magnetical alignability and provides a bilayered structure in the physiologically relevant conditions [1]. As a result, it is commonly used as a "goniometric" substrate for solid-state NMR studies to resolve membrane proteins' structures [2–7]. Bicellar mixtures also have had various applications in other research areas, e.g., crystallization of membrane proteins [8–12], solution NMR study on membrane proteins [13–18], pharmaceutical [19,20] and skin care products [21–24].

Many bicellar mixtures composed of zwitterionic long-chain dimyristoyl (di-C_{14}) and short-chain dihexanoyl (di-C_6) phosphatidylcholine (DMPC and DHPC) have been reported mainly because their magnetically alignable phase (presumably ribbons or lamellae) takes place at physiologically relevant temperatures. This alignable phase normally forms at a temperature higher than the melting transition temperature, T_M of the long-chain lipid (in this case, 23 °C for DMPC) [1–7]. Therefore, aligning bicellar mixtures composed of longer chain lipids, which have a higher T_M, may risk denaturing the associated proteins. In the past, detailed spontaneous structural diagrams of DMPC/DHPC have been studied using cryogenic transmission electron microscopy (cryo-TEM) [25,26], small angle neutron scattering (SANS) [27–30], and NMR [31–33]. The current consensus among these studies is that perforated magnetically-alignable (or ribbon-meshed) lamellae form in the high lipid concentration (C_{lp}) samples at temperature a few degrees C higher than T_M of DMPC, while nanodiscs and bilayered ribbons are commonly found at low C_{lp} and low temperatures. In spite of extensive investigations on the DMPC/DHPC systems, most of them involve high C_{lp} for the purpose of membrane alignment or stronger signals from the studied proteins associated with the bilayers. Very few studies that focus on the low-concentration (<1.0 wt.%) bicellar mixtures are

* Corresponding author at: Institute of Materials Science, Dept. Chemical & Biomolecular Engineering, Dept. Biomedical Engineering, UConn, Storrs, CT 06269, USA.
E-mail address: mu-ping.nieh@ims.uconn.edu (M.-P. Nieh).

http://dx.doi.org/10.1016/j.bbamem.2014.02.004
0005-2736/Published by Elsevier B.V.

reported for their potential applications as nano-carriers for pharmaceuticals [20,34–37]. It should also be noted that a charged long-chain dimyristoyl phosphatidylglycerol (DMPG) is commonly added in the DMPC/DHPC mixture to stabilize the disc-like bicelles (nanodiscs) at low C_{lp} [27,38–40], presumably due to strong Coulombic interactions.

Upon elevation of temperature, a nanodisc-to-vesicle transition can occur in the low-C_{lp} DMPC/DHPC/DMPG mixture [34,35]. Both nanodiscs and unilamellar vesicles (ULVs) normally have low polydispersities with a standard deviation <25% [34–37] — an important feature for many applications. For biomedical purpose, the spontaneously forming uniform nanodiscs and ULVs can be used as in vivo nano-carriers to entrap hydrophobic and hydrophilic molecules, respectively. Therefore, their stability in terms of temperature, C_{lp}, and physiologically relevant salinity are crucial. The nanodisc-to-ULV structural transition temperature ties with the T_M of DMPC, presumably due to the increased line tension at disc rim caused by the enhanced miscibility between DMPC and DHPC when both are in the L_α phase. In order to have stable in vivo nanodiscs, the T_M of the long-chain lipid needs to be higher than 37 °C. A candidate zwitterionic long-chain lipid is dipalmitoyl (di-C_{16}) phosphatidylcholine (DPPC), whose T_M is around 41 °C. In fact, the DPPC/DHPC mixture, though is not as extensively studied as DMPC/DHPC, has already been reported in literature [22,23,41–43]. Some simulation work has also been performed on DPPC bicellar mixtures using coarse-grain molecular dynamics [44–46] and atomic approach [47]. However, to the best of our knowledge, self-assembled structures of DPPC/DHPC mixtures doped with a charged dipalmitoyl (di-C_{16}) phosphatidylglycerol (DPPG) have not yet been investigated. It is expected that the addition of DPPG should stabilize the nanodiscs because of the enhanced Coulombic interaction [40].

In order to prolong the in vivo circulation, a general approach is to graft polyethylene glycol (PEG) on the surface of nanoparticles (NPs) [48,49], leading to the reduction of the uptake of NPs through reticuloendothelial system (RES). For lipid mixtures, PEG conjugated (PEGylated) lipids are commonly used to achieve this purpose. In this case, a common PEGylated lipid, distearoyl phosphoethanolamine-N-[methoxy (polyethylene glycol)-2000] (PEG2000-DSPE), is added in the bicellar mixtures and its effect on the spontaneous morphology is investigated.

There are several aims to be achieved in this paper. First, the applicability of the self-assembly principle in the DMPC/DHPC bicellar mixtures will be examined for the DPPC/DHPC mixture, including the formation of uniform nanodiscs and uniform nano-ULVs at temperatures lower and higher than T_M of DPPC, respectively. The reversibility of the low-T structure will also be investigated as the temperature varies from low ($<T_M$) to high ($>T_M$) where the nanodisc-to-vesicle structural transformation is expected to take place, and then back to low. Furthermore, the effects of C_{lp} and salinity (in the presence of PBS solution) on the structures will be studied to understand the stability of the nanoparticles. Finally, the effect of additional PEGylated lipid on the spontaneous structure will be evaluated. All the detailed morphologies are identified by SANS while the stability of the self-assembled nanodiscs is examined using dynamic light scattering (DLS).

2. Materials and methods

2.1. Materials

DPPC, DHPC, DPPG and PEG2000-DSPE were purchased from Avanti Polar Lipids (Alabaster, AL, USA) and used without further purification. Powder of phosphate buffered saline (PBS) was purchased from Sigma-Aldrich (St. Louis, MO). Deuterium oxide (99.9%) was purchased from Cambridge Isotope Co. The PBS solution was prepared by dissolving 9.38 g of the powder into 1 L of D_2O to form a final composition of 137 mM NaCl, 2.7 mM KCl, 10 mM Na_2HPO_4. Two series of samples with identical concentrations were prepared individually in D_2O or PBS solution. Light (H_2O) and heavy (D_2O) waters were used for DLS and SANS measurements, respectively. The compositions of all samples have been shown in Table 1, resulting in three constant molar ratios of $\frac{[DPPC]+[DPPG]+[PEG2000-DSPE]}{[DHPC]}$ (i.e., the long- to short-chain lipid molar ratio, Q), $\frac{[DPPG]}{[DPPC]+[DPPG]+[PEG2000-DSPE]}$ (i.e., the charged long- to total long-chain lipid molar ratio, R) and $\frac{[PEG2000-DSPE]}{[\text{total lipids}]}$ (i.e., the PEG2000-DSPE to total lipid molar ratio, P) to be 3, 0.05 and 0.05, respectively, in order to compare with the result of the DMPC/DHPC/DMPG system in the absence of the PEGylated lipid reported previously [27,29,30].

Table 1
Composition of individual lipids in aqueous solutions (in mol%).

DPPC	71.25	66.25
DHPC	25.00	25.00
DPPG	3.75	3.75
PEG2000-DSPE	0	5.00

The dry lipids were first weighted and then dispersed in filtered D.I. water (or D_2O for SANS) or PBS solutions (or PBS/D_2O for SANS) to form stock solutions with an initial total lipid concentration of 200.0 mg/mL. After successive vortex and temperature cycling between 25 and 60 °C, the lipid stock solutions were homogenously dissolved in all cases (transparent at room temperature and below). The stock solutions were then progressively diluted at room temperature to the final solutions with total lipid concentrations of 100, 10 and 1 mg/mL, respectively.

2.2. SANS

SANS data were collected using the EQ-SANS instrument at the Spallation Neutron Source of Oak Ridge National Laboratory. The sample-to-detector distance was set to 4.0 m. A 25 mm source aperture and a 10 mm sample aperture were used to collimate the incident beam. The instrument was operated in the 30 Hz "frame-skipping" mode with a minimum wavelength setting of 2.5 Å, providing a second wavelength band starting at 9.4 Å resulting in a combined q-range ($q = \frac{4\pi}{\lambda}\sin\frac{\theta}{2}$, where θ is the scattering angle and λ is the neutron wavelength) that covered 0.007–0.40 $Å^{-1}$ for data reduction and analysis. The useful q range provided by the data fitting was from 0.007 to 0.25 $Å^{-1}$. Data correction followed standard procedures implemented in MantidPlot (http://www.mantidproject.org/) to correct for sample transmission, detector sensitivity, and dark background before circularly averaging the 2D data around the beam center to produce I (q) versus q. The data from the two wavelength bands were merged into a single profile using MantidPlot. The reduced SANS data were then best fitted with appropriate models provided at NIST (National Institute of Standards and Technology) Center for Neutron Research (NCNR) in the format of IGOR-PRO program [50,51].

2.3. Dynamic light scattering

The light scattering instrument is an ALV compact goniometer system with multi-detectors (CGS-3MD) (Germany), which consists of a 22 mW He–Ne laser (emitting vertically polarized light with a wavelength of 632.8 nm) and four avalanche photo diode (APD) detectors, which are equally spaced out (32° apart) on an arc of a tray driven by a goniometer. Both static and dynamic light scattering (SLS and DLS) data can be collected simultaneously. One of the four detectors have a sample and a reference output, allowing pseudo-cross correlation measurements (single detector mode) thus yielding better data quality in the range of fast decay time (τ). The auto- or cross-correlation function is collected by an ALV-7004 digital multiple tau real time correlator, yielding data in the range as short as 25 ns. In this experiment, the

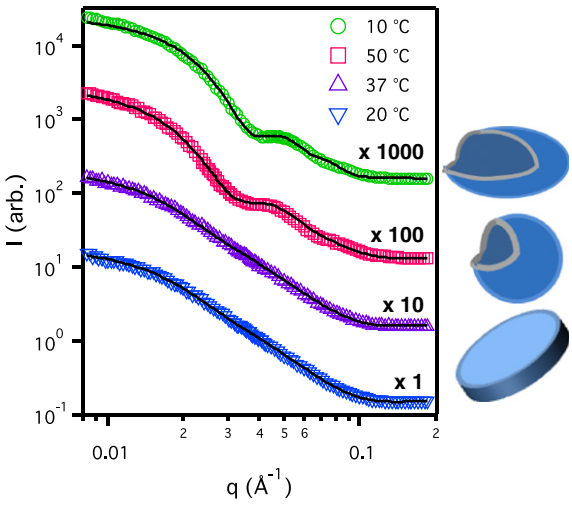

Fig. 1. The SANS data of 1 mg/mL DPPC/DHPC/DPPG solution at different temperatures following the thermal sequence: from 20 (tip-down triangles), 37(tip-up triangles), 50 (squares) to 10 (circles) °C. The solid curves are the best fits. The SANS data are rescaled by a factor (from 1 to 1000) to enhance the visual clarity.

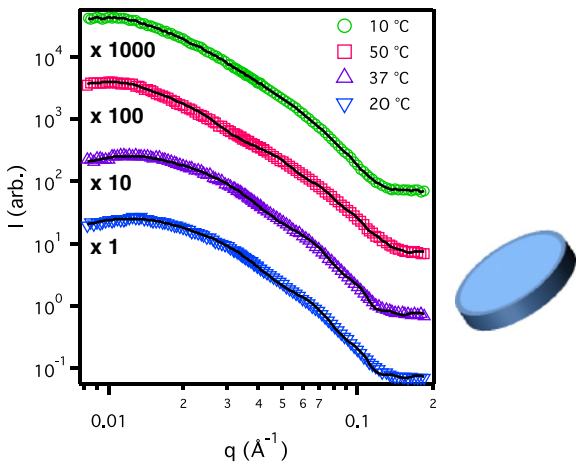

Fig. 2. The SANS data of 10 mg/mL DPPC/DHPC/DPPG solution at different temperatures following the thermal sequence: from 20 (tip-down triangles), 37 (tip-up triangles), 50 (squares) to 10 (circles) °C. The solid curves are the best fits. The SANS data are rescaled by a factor (from 1 to 1000) to enhance the visual clarity.

DLS data were obtained from the cross-correlation function using the single detector mode.

For single-sized system the intensity correlation function can be described as a single exponential decay with a rate constant Γ: $e^{-2\Gamma\tau}$. As a result, the translational diffusion coefficient, D can be related with Γ with a simple function, $D = \Gamma / q^2$, where the magnitude of the scattering vector is $q = \frac{4n\pi}{\lambda} \sin\frac{\theta}{2}$ and n is the refractive index of the solution. In this report, the scattering angle, θ was always set at 90°. Based on the Stokes–Einstein relation, the hydrodynamic radius, R_H, can be related with D of a uniform-sized spherical particle: $R_H = \frac{k_B T}{6\pi\eta D}$, where k_B and η are the Boltzmann constant and the viscosity of the solvent (H_2O in this case), respectively. If the system contains more than one size of particles, the time correlation function will indicate multimodal decays deviating from the single exponential decay. The ALV software is able to resolve multimodal distribution functions yielding multimodal distributions of R_H through CONTIN procedure.

2.4. Negatively staining TEM

The negatively staining TEM micrograph was obtained by a FEI Tecnai T12 transmission electron microscope. The samples were prepared in the following steps. A drop of 5 μL solution in concentration of 0.01 mg/mL was first placed on a 400 mesh copper grid coated with Formvar/carbon film (Electron Microscopy Sciences, PA, USA). Excessive solution was then blotted with Whatman filter paper. Then, the sample was negatively stained with 5 μL of 10 mg/mL Uranyl acetate (SPI Supplies, PA, USA) and the excessive staining solution was again removed with the filter paper. In the cases of PBS solutions, the grids were rinsed by water twice before staining in order to reduce the possible artifact caused by the interaction between phosphate salt and Uranyl acetate. Afterwards, the grid was dried at room temperature. Electron micrographs were taken at an accelerating voltage of 80 kV.

3. Results

It has been reported that nanodisc-to-ULV transition can take place in the lipid mixtures made of DMPC/DHPC/DMPG upon elevation of temperature in the absence of PEGylated lipid [1]. To investigate whether the same transition takes place in a DPPC/DHPC/DPPG solution under a similar condition, SANS measurements were conducted as a function of temperature and the data of the sample with a total lipid concentration, C_{lp} of 1 mg/mL are shown in Fig. 1. The temperature follows a thermal sequence: 20, 37, 50 and then 10 °C. The two initial SANS data at 20 and 37 °C have a common feature that reveals an intensity plateau at low-q and a monotonic decay at high-q. This SANS pattern can be best fit using a polydispersed radius disc (PRD) model (supplementary data). The best-fit thickness (48 Å) of the nanodiscs (Table 2) is consistent with the DPPC bilayer thickness in the low-T crystal (below 24.8 °C) and gel phases (below 41 °C) as reported by Nagle et al.: 48.2 and 47.2 Å, respectively [52]. The fact that the same SANS pattern is observed indicates that the morphology of disc remains until the temperature exceeds the T_M of DPPC, although several pre-transition phases (e.g., crystal, ripple phases) have been reported in the case of pure DPPC [53]. Furthermore, the result of differential scanning calorimetry applied to the sample shows that only single transition (presumably from gel to L_α) is observed in this case though the T_M is ~2 °C higher than the typical T_M of pure DPPC (supplementary data), implicative of single structural transition.

The radius of the nanodiscs increases slightly from 123 to 134 Å (Table 2), possibly due to the migration of rim DHPC to DPPC-rich bilayered region as their miscibility increases with increased T, resulting in the increase of line tension at the rim and hence leading to the disc

Table 2
Parameters of various models that best fit the SANS data of 1 mg/mL DPPC/DHPC/DPPG in D_2O at different temperatures.

T, °C	20	37	50		10	
Models	PRD	PRD	PSSS		OSS	
Radius, Å	123 ± 8	134 ± 10	Inner radius, Å	70 ± 2	Inner major axis Inner minor Axis	64 ± 3 35 ± 2
Thickness, Å	48 ± 1	48 ± 1	Shell thickness, Å	38 ± 1	Outer major axis Outer minor axis	126 ± 2 70 ± 2
Polydispersity Volume, Å^3	0.22 ± 0.10 2.3×10^6	0.21 ± 0.10 2.7×10^6	Inner radius polydispersity 3.8×10^6	0.27 ± 0.10	– 4.0×10^6	

Table 3
Parameters of the PRD combined with Hayter–Penfold structure factor model that best fits the SANS data of 10 mg/mL DPPC/DHPC/DPPG in D_2O at different temperatures.

T, °C	20	37	50	10
Model	PRD + Hayter–Penfold structure factor			
Radius, Å	87.0 ± 1.0	89.0 ± 1.0	124.0 ± 1.0	118.0 ± 2.0
Thickness, Å	47 ± 1	46 ± 1	39.0 ± 1	46 ± 1
Charge number	15.1 ± 6	18.2 ± 6	23 ± 5	25.0 ± 5
Volume, Å^3	1.11 × 10^6	1.14 × 10^6	1.88 × 10^6	2.01 × 10^6

coalescence [37,54]. Continuous increase of temperature to 50 °C results in the expected disc-to-vesicle transition, where the SANS curve contains broad peaks – a characteristic of the scattering pattern of low-polydispersity ULV – and thus can be best fit by a polydisperse single-shell spherical (PSSS) model (supplementary data). The best fit shell (bilayer) thickness (38 Å) of the vesicles was found ~10 Å less than that in the low-T cases presumably due to the melting of the acyl chain (in L_α phase), consistent with a previous report [52,55].

However, the initial discoidal morphology did not reoccur as T dropped to 10 °C. Instead, the spherical vesicles were deformed into oblate shape according to the best-fit result using oblate single-shell (OSS) model (supplementary data). The same irreversible process was also observed previously in a similar system composed of DMPC/DHPC/DMPG solution at a low C_{lp} [34,35]. The best-fit shell thickness along the minor axis (35 Å) was even less than the spherical shell thickness at 50 °C, while the best-fit shell thickness along the major axis is thicker (>60 Å). At this temperature, DPPC was supposed to be in the gel phase where thicker bilayer is expected. The best fitting result implies that lipid segregation may occur in the case of oblate vesicles where DHPC and DPPC preferred to be located the quadrants around minor and major axes, respectively. This can be caused by the mismatch between DPPC and DHPC and packing stress leading to the segregation or even perforation as proposed in literature [56].

With a tenfold increase of C_{lp} (i.e., 10 mg/mL), the structural transition behaves differently from what has been observed in the low-C_{lp} sample as shown in Fig. 2. The sample underwent the same heating sequence, i.e., 20, 37, 50 °C and then to 10 °C. All of the SANS curves have a broad peak between 0.007 and 0.02 Å^{-1}, indicating a structure factor due to moderate Coulombic interaction, followed by a monotonic decay at the higher q range. Therefore, a discoidal model combined with Hayter–Penfold structure factor (supplementary data) was applied to fit

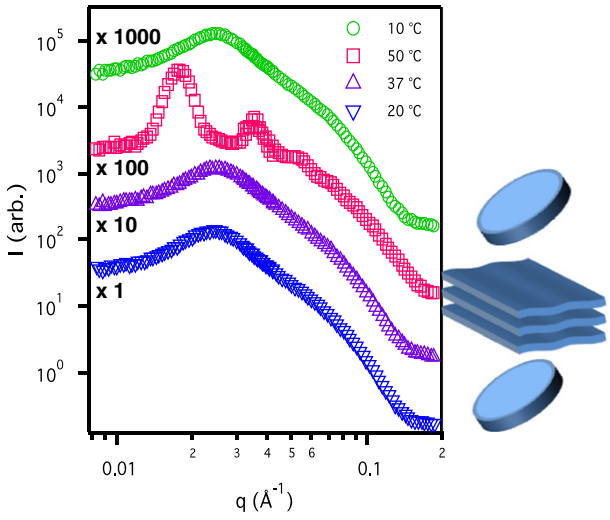

Fig. 3. The SANS data of 100 mg/mL DPPC/DHPC/DPPG solution at different temperatures following the thermal sequence: from 20 (tip-down triangles), 37(tip-up triangles), 50 (squares) to 10 (circles) °C. The SANS data are rescaled by a factor (from 1 to 1000) to enhance the visual clarity.

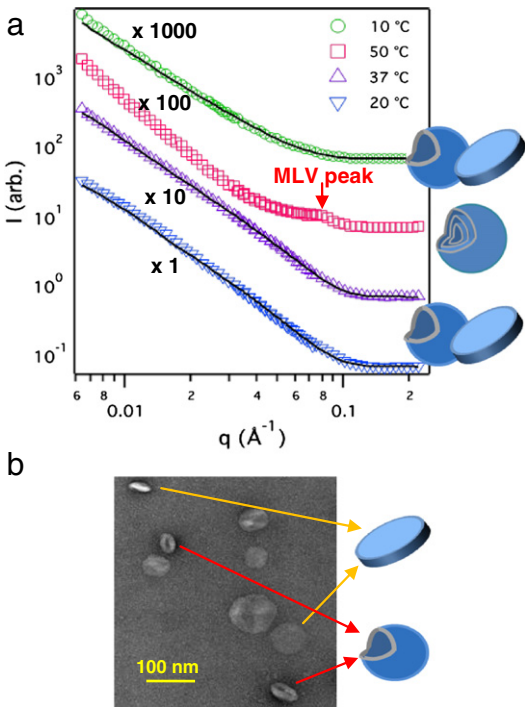

Fig. 4. (a) The SANS data of 1.0 mg/mL DPPC/DHPC/DPPG in PBS solution at different temperatures following the thermal sequence: from 20 (tip-down triangles), 37(tip-up triangles), 50 (squares) to 10 (circles) °C. The solid curves are the best fits. The SANS data are rescaled by a factor (from 1 to 1000) to enhance the visual clarity. (b) The TEM micrograph of 20 °C sample, where large discs (both top and side views) and possibly ruptured vesicles are observed.

the SANS data. The fact that no evident nanodisc-to-vesicle transition occurs upon increasing T is consistent with a previous report, where a highly charged DMPC/DMPG/DHPC mixture also did not exhibit such structural transition upon elevation of temperature above T_M of DMPC [27], presumably due to the interplay between a strong Coulombic interaction and sufficient DHPC that stabilizes the disc rim. The only apparent difference in SANS pattern upon the elevation of T to 50 °C is the shift of the broad peak toward lower q, indicative of an increased spacing between nanodiscs caused by the disc coalescence. The best fitting parameters also illustrate increased radii of the discs from 88 Å to 124 Å as T increases from 20 to 50 °C (Table 3). Moreover, a decrease in disc thickness (from 47 to 39 Å) confirms the transition of DPPC from gel to L_α phase. It should be noted that the disc volume increases from 1110 to 1880 nm^3 as T increases from 20 to 50 °C and then remains practically unchanged as the sample was cooled back to 10 °C from 50 °C (with a difference less that 10%), indicative of the irreversibility of the nanodiscs. Nevertheless, the best-fitting thickness of the reentering 10 °C discs after the T-cycle is consistent with that of the gel-phase DPPC.

SANS data of an even higher C_{lp} (e.g., 100 mg/mL) sample (Fig. 3) exhibit similar temperature dependence as reported in the DMPC/DMPG/DHPC system [27]. The scattering patterns at low temperatures (i.e., ≤37 °C) are practically identical and can be characterized by PRD

Table 4
Parameters of the PRD model that best fits the SANS data of 1 mg/mL DPPC/DHPC/DPPG in PBS buffer at different temperatures.

T, °C	20	37	50	10
Models	PRD		MLVs	PRD
Radius, Å	>300	>300	–	>300
Thickness, Å	47.2 ± 1	45.2 ± 1	–	47.5 ± 1
Polydispersity	0.12 ± 0.10	0.13 ± 0.10		0.10 ± 0.10

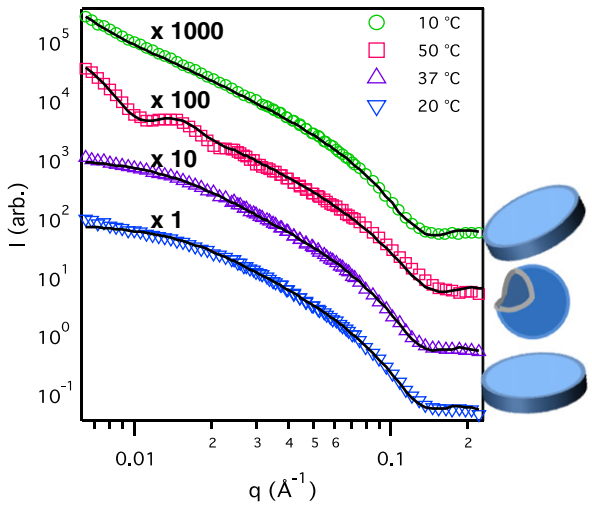

Fig. 5. The SANS data of 10 mg/mL DPPC/DHPC/DPPG in the PBS solution at different temperatures following the thermal sequence: from 20 (tip-down triangles), 37(tip-up triangles), 50 (squares) to 10 (circles) °C. The solid curves are the best fits. The SANS data are rescaled by a factor (from 1 to 1000) to enhance the visual clarity.

with a strong structure factor, indicative of no temperature dependence. At T = 50 °C, the scattering pattern transformed into many high-order quasi-Bragg reflections (more than 3 peaks), indicative of a regular-spaced lamellar phase. It is noteworthy that unlike the low-C_{lp} samples the scattering pattern was fully recovered (almost identical as the ones at 20 and 37 °C) after the sample reentered 10 °C. The reversibility of the high-C_{lp} sample proves the validity for the repeated temperature cycling in the protocol of sample preparation, i.e., the morphology of the self-assembly not affected by the thermal path.

In order to understand the effect of salinity on the morphology of aggregates, SANS measurements were conducted on the 1.0 mg/mL samples prepared in PBS/D_2O undergoing a similar thermal path in the sequence of 20, 37, 50 and 10 °C [as shown in Fig. 4(a)]. A significant effect of PBS on the scattering patterns is found as compared with those in Fig. 1. The lack of intensity plateau at low q indicates the existence of larger particles. Negatively-staining TEM micrograph was taken on a low-T (i.e., 20 °C) sample [Fig. 4(b)] revealing large, polydisperse discs and possibly ruptured vesicles (due to the drying process), consistent with the observed low-q intensity upturn in the SANS patterns. Since both large discs and vesicles have a common basic bilayered lamellar structure, the PRD model can be used to describe the SANS data of the sample which may contain a mixture of discs and vesicles at 20 and 37 °C. As expected, the best-fitting radii only provide the minimum value (>300 Å), while the best-fitting bilayered thicknesses (between 45 and 48 Å) remain valid.

At 50 °C, a quasi-Bragg peak at q = 0.0085 Å^{-1}, corresponding to a repeat d-spacing of 73.9 Å, appears. This spacing is typically found in the case of non-swellable lamellar domains, consistent with the result of a previous study on weakly-charged or high-salinity DMPC/DHPC/DMPG solutions at high temperature, where multi-lamellar vesicles (MLVs) were observed [39]. The negatively-staining TEM was not applied to identify the MLV structure at high T because of inaccessibility of cryogenic TEM. However, the MLV peak provides unambiguous evidence. The formation of MLVs can be rationalized by the enhanced interaction between nanodiscs as the charges on the bilayers are significantly screened by the PBS salt. As temperature dropped from 50 to 10 °C, the MLV peak disappears, indicating the unbinding of the multi-lamellarity. The SANS data can be again best-fit with the PRD model, indicating large discoidal or/and vesicular morphology. The best-fitting radii are again outside the probing range of the SANS setup (judging by no tendency of the low-q plateau). All the best-fit parameters are listed in Table 4.

The same experimental procedure was applied to a higher-C_{lp} sample (i.e., 10 mg/mL) as shown in Fig. 5. In contrast to the lower C_{lp} sample (Fig. 4), the SANS data indicate typical scattering patterns of nanodiscs at 20 and 37 °C with radii (95–120 Å) slightly larger than those in the absence of PBS (Table 3). Moreover at 50 °C, instead of MLV, a characteristic pattern of ULV with an average inner radius of 253 Å (>3 times of the size of the ULV found in the 1 mg/mL, 50 °C sample in the absence of PBS as illustrated in Table 2) and a slightly thinner bilayer thickness (~36.5 Å) was observed. After the sample was cooled back to 10 °C, the discoidal morphology and the thickness of the bilayer (according to model fitting) seemed to recover, while the radius (~410 Å) became significantly larger than the ones before heating (Table 5). In fact, the lacking of a low-q plateau makes it difficult to accurately determine the radius of the reentering nanodiscs. The result suggests that high-C_{lp} sample enhances the stability of the discs as well as the reversibility of the system. This is also observed in the system in the absence of PBS (Fig. 2).

The uptake of nanoparticles by RES can be reduced as their surface is modified with PEG chains, resulting in lengthened in vivo circulation half-life of the nanoparticles [48,49]. In this study, 5.0 mol% of PEG2000-DSPE is incorporated with the nanodiscs to enhance the stability of the NPs. Fig. 6(a) shows the SANS data of a 1.0 mg/mL solution of DPPC/DPPG/DHPC/PEG2000-DSPE in D_2O at 10, 37 and 67 °C. The scattering patterns of all the samples indicate the nanodisc morphology throughout the studied temperatures, indicating a high structural stability of the nanodiscs induced by PEG2000-DSPE. A negatively staining TEM image of the sample as shown in Fig. 6(b) further confirms the SANS data. The best fitting radius increases slightly (from 76 to 92 Å) as T increases from 10 to 67 °C (Table 6). It should be noted that the SANS data were collected at a different instrument, CG3-BioSANS (at High Flux Isotope Reactor), which has a different instrument resolution which may affect the best-fitting results. This may partially explain the apparent increase in disc thickness (~70 Å) at low T compared to that in the absence of PEG-DSPE (~48 Å in Table 2). However, it is also possible that the majority of PEG2000-DSPE may locate at the bilayered planar region of the nanodiscs with the PEG chains extending toward the water phase. Recently, a coarse-grain molecular dynamic simulation indicates that PEGylated lipid may prefer to locate at the rim in a similar system (in the absence of DHPC) because of the high spontaneous curvature attributed to the large head group [45]. As a result, the immiscibility between L_α DHPC and gel DPPC was not considered in the simulation. This may explain the difference between simulated result and experimental data. As T increases to 67 °C, the disc thickness decreases to 60 Å (Table 6), possibly due to the combinational effects

Table 5
Parameters of the models that best fit the SANS data of 10 mg/mL DPPC/DHPC/DPPG sample in PBS buffer at different temperatures.

T, °C	20	37	50		10	
Models	PRD		PSSS		PRD	
Radius, Å	95 ± 1	112 ± 1	Inner radius, Å	253 ± 1	Radius, Å	410 ± 40
Thickness, Å	46 ± 1	46 ± 1	Shell thickness, Å	36 ± 1	Thickness, Å	44 ± 1
Polydispersity	0.34	0.33	0.25		0.30	
Volume, Å^3	1.3×10^6	1.8×10^6	3.4×10^7		2.3×10^7	

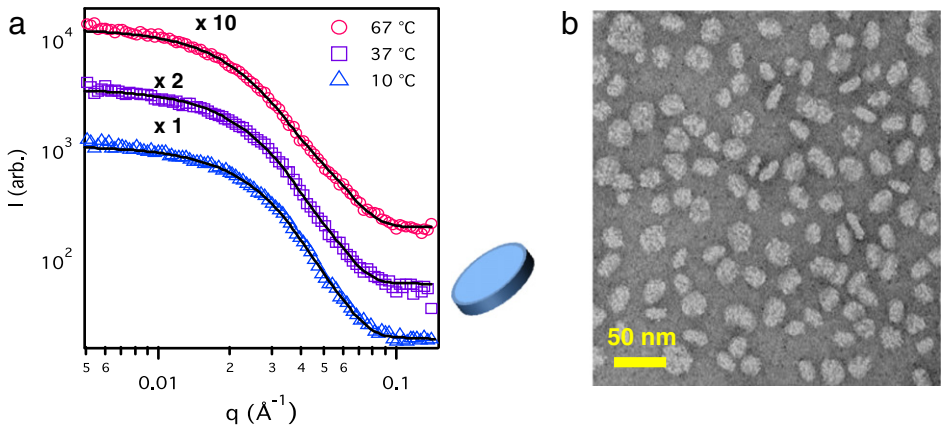

Fig. 6. (a) The SANS data of 1 mg/mL DPPC/DHPC/DPPG/PEG2000-DSPE in D2O at different temperatures following the thermal sequence: from 10 (triangles), 37 (squares), 67 (circles) °C, The solid curves are the best fits. The SANS data are rescaled by a factor (from 1 to 2 to 10) to enhance the visual clarity. (b) The negatively staining TEM micrograph is obtained from the sample of a concentration of 0.01 mg/mL.

of the transition of DPPC from gel to L_α phase (as observed earlier) and the collapse of the PEG at a high temperature caused by the disruption of hydrogen bonds [57].

To investigate the effect of C_{lp} on the morphology in the presence of PEG2000-DSPE, the SANS data of 10 mg/mL mixture containing PEG2000-DSPE in D_2O at 10, 37 and 67 °C are shown in Fig. 7. All of the SANS curves have the characteristic feature described by the discoidal model with a Hayter–Penfold structure factor [58], consistent with what was observed in Fig. 2, where nanodiscs were stable throughout the temperature range (from 10 to 67 °C). The radii of the nanodiscs are comparable to those in the low-C_{lp} samples at the corresponding temperatures. As the DPPC underwent the phase transition from gel (10 °C) to L_α phase (67 °C), the radius of the discs slightly increased from 75 to 90 Å and the thickness of the discs decreased from 50 to 39 Å (Table 7). However, the volume seems to remain practically the same or slightly increase (within 10%), indicating that the PEG2000-DSPE may effectively inhibit the disc coalescence, which takes place at the systems in absence of PEG2000-DSPE (with ~80% increase in volume as shown in Table 3). The radii of nanodiscs are also found smaller than those at the corresponding temperature in the absence of PEG2000-DSPE (Table 3).

The stability of these nanodiscs was also investigated under physiologically relevant high-salinity condition in the presence of PBS. The 1.0 mg/mL DPPC/DHPC/DPPG/PEG-DSPE in PBS buffer underwent the same thermal path as did the previous samples in the sequence of 20, 37, 50 and 10 °C. The two sets of SANS data (Fig. 8) obtained at the initial low temperatures (20 and 37 °C) are similar to each other and can be best fit with the PRD model. The best fitting parameters of the PRD model to the SANS data are listed in Table 8. The best fitting radii of the nanodiscs are larger than those in water (see Table 7) at the corresponding temperatures, indicating that PBS effectively screens the interparticle Coulombic repulsion, thus promoting the coalescence among discs. Nevertheless, when compared with the sample in the absence of PEG2000-DSPE (in PBS) at the corresponding C_{lp} and temperatures (Fig. 4), where polydispersed large discs and vesicles were observed, the PEG2000-DSPE shows significant enhancement in the stability of the nanodiscs, inhibiting the coalescence of discs. Upon the elevation of temperature to 50 °C, several oscillations are found in the scattering pattern. The SANS curve, though similar to those of the spherical vesicles, cannot be described by PSSS model. Only OSS model can fit the data with reasonable agreement. These oblate vesicles were stable even as the temperature dropped to 10 °C, where a smaller size but a similar shell volume was observed based on the best-fit parameters, indicating that the morphology and aggregation number do not alter after the system reenters to the lower temperature. Oblate vesicles have also been found in a low-C_{lp} DMPC/DHPC/DMPG system [35].

Quantitative analysis on the parameters obtained from the best-fit results provides further insight to the system. First, similar to all the other aforementioned nanodiscs, the radius of nanodiscs slightly increased (from 96 to 106 Å) with increased T (from 20 to 37 °C) presumably due to the coalescence process. In regard to the oblate vesicles forming at 50 °C, a substantially thinner shell thickness along the minor than the major axis was observed (69 Å versus 14 Å) in comparison with that of 1.0 mg/mL DPPC/DHPC/DPPG in D_2O (62 Å versus 35 Å in Table 2) reentering 10 °C. The non-uniform thickness suggests that the long-chain DPPC and PEG-2000 DSPE might not locate themselves on the quadrants along the minor axis. It is even possible that holes, whose edge is stabilized by DHPC, might form along the minor axis

Table 6
Parameters of the PRD model that best fits the SANS data of 1 mg/mL DPPC/DHPC/DPPG/PEG2000-DSPE in D_2O at different temperatures.

T, °C	10	37	67
Model	PRD		
Radius, Å	76 ± 1	83 ± 1	92 ± 1
Thickness, Å	70 ± 1	70 ± 1	60 ± 1
Polydispersity	0.2	0.2	0.2
Volume, Å^3	1.27 × 10^6	1.52 × 10^6	1.58 × 10^6

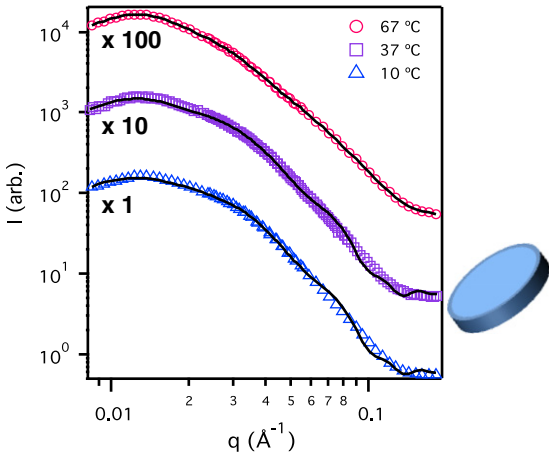

Fig. 7. The SANS data of 10 mg/mL DPPC/DHPC/DPPG/PEG2000-DSPE in D2O at different temperatures following the thermal sequence: from 10 (triangles), 37(squares), 67 (circles) °C. The solid curves are the best fits. The SANS data are rescaled by a factor (from 1 to 100) to enhance the visual clarity.

Table 7
Parameters of the PRD model combined with Hayter–Penfold structure factor that best fits the SANS data of 10 mg/mL DPPC/DHPC/DPPG/PEG2000-DSPE in D_2O at different temperatures.

T, °C	10	37	67
models	PRD + Hayter/Penfold structure factor		
Radius, Å	75 ± 1	76 ± 1	90 ± 1
Thickness, Å	50 ± 1	50 ± 1	39 ± 1
Volume, Å^3	8.60 × 10^5	9.07 × 10^5	9.82 × 10^5

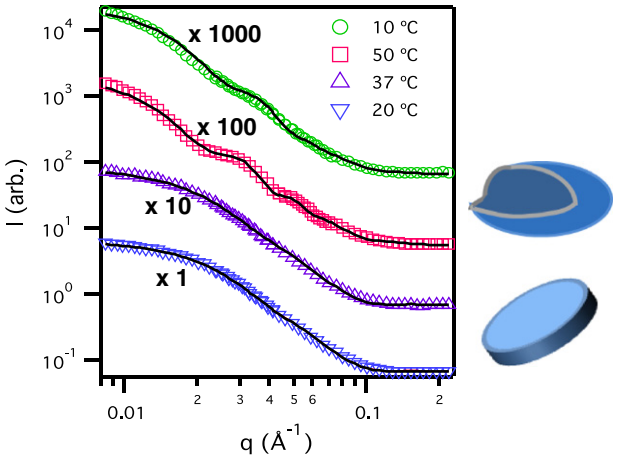

Fig. 8. The SANS data of 1.0 mg/mL DPPC/DHPC/DPPG/PEG2000-DSPE in the PBS buffer at different temperatures following the following thermal sequence: from 20 (tip-down triangles), 37 (tip-up triangles), 50(squares) and back to 10 (circles) °C. The solid curves are the best fits. The SANS data are rescaled by a factor (from 1 to 1000) for better visual clarity.

as described in literature [59]. The oblate vesicles as reentering low T (10 °C) yield a thicker bilayer along both minor (22 Å) and major axes (81 Å), possibly due to the combination effect of gel phase of DPPC and extended PEG chains due to the reduction of temperature.

Regarding the sample of a higher C_{lp}, (10 mg/mL), nanodiscs were found at low temperatures (10 and 37 °C) as anticipated (Fig. 9). Their dimensions (radii and thickness) are similar to those in the low-C_{lp} samples at the corresponding T. At high T (67 °C), instead of OSS model being required for fitting in the case of 1 mg/mL sample, the PSSS model is sufficient to fit the SANS data yielding a good agreement, indicative of the formation of spherical vesicles. This result suggests that the spherical structure is preserved in the higher-C_{lp} sample possibly due to a more homogeneous distribution of the species on the bilayer. Two possibilities are likely attributed to the homogeneity: (1) the temperature of the 10 mg/mL sample (67 °C) is higher than that in the low-C_{lp} (1 mg/mL) sample (50 °C), (2) more DHPC on the bilayer (assuming a constant concentration of the free DHPC in solution) enhances the homogeneity. More experiments will be designed to further investigate this effect of C_{lp} on different morphologies. The best-fit parameters of all the models used are illustrated in Table 9.

4. Discussion

4.1. Temperature effect

The spontaneous structures of DPPC/DHPC/DPPG mixture as a function of T and C_{lp} are similar to those of the DMPC/DHPC/DMPG in literature [54] where the structural transition temperature was found closely correlating with the melting transition temperature, T_M, of the long-chain lipid, in this case, DPPC and DPPG (i.e., 41 °C). Below T_M, the long-chain DPPC, DPPG (in gel phase) and the short-chain DHPC (in L_α phase) segregate from each other forming the planar bilayered and the rim of the nanodiscs, respectively. As T increases above T_M, DPPC melts into the L_α phase and becomes miscible with DHPC, promoting the migration of rim DHPC to the bilayered region, consequently resulting in insufficient rim DHPC. This migration causes increased line tension at the rim and instability of the nanodiscs, leading to coalescence of the discs and eventually folding into ULVs [54]. The disc-to-vesicle transition is depicted as Fig. 10(a), (b) and (d) in all low-C_{lp} and some higher-C_{lp} samples as well as has been reported in other DMPC-containing systems in literature [60,61]. An early study on a melittin/DPPC system using DLS and TEM also showed a disc-to-vesicle transition as T went across T_M [62], suggesting that melittin may play a similar role as the short-chain lipid. The current system confirms the universality of such transformation with different lipids or peptides.

4.2. C_{lp} effect

In regard to samples of various C_{lp} (i.e., comparing 1.0 mg/mL with 10 mg/mL samples), three significant effects observed due to the higher C_{lp} are also summarized in Fig. 10. (1) Discoidal structure is more stabilized at high T (50 °C) as shown in Figs. 1 and 2 [also Fig. 10 (a)] at the current charge density. (2) In presence of PBS, high-C_{lp} samples inhibit the formation of MLVs [Figs. 4, 5 and 10(b)]. (3) High C_{lp} also promotes the spherical instead of oblate shape in the presence of salt and PEG2000-DSPE as shown in Figs. 8, 9 and 10 (d).

All the above-mentioned observations can be rationalized by the available free DHPC molecules in solution. Since the composition of the lipid mixture remains unaltered in the samples of the two different C_{lpS} in the same series, dilution should have exerted no effect on the lipid composition of the nanoparticles (NPs) but only increased the interparticle spacing. Nevertheless, it should be noted that the critical micelle concentration of pure DHPC is 15 mM, which is ~3 × 10^7 higher than that of DPPC (i.e., 0.46 nM) [63]. Dilution effectively reduces the concentrations of all the free lipids in solution and consequently perturbs their pseudo-equilibrium between the lipids associated with the NPs and the free ones. The mismatched solubility of different lipids results in different degrees of perturbation in the pseudo-equilibrium states. As a result, more highly-soluble lipids (DHPC in this case) will be "pulled" out of the NPs upon dilution,

Table 8
Parameters of various models that best fit the SANS data of 1 mg/mL DPPC/DHPC/DPPG/PEG2000-DSPE in PBS buffer at different temperatures.

T, °C	20	37		50	10
Models	PRD		OSS		
Radius, Å	96 ± 3	105 ± 3	Major core semi-axis, Å	123 ± 3	90 ± 1
			Minor core semi-axis, Å	46 ± 3	37 ± 2
Thickness, Å	54 ± 1	54 ± 1	Major shell semi-axis, Å	192 ± 3	171 ± 2
			Minor shell semi-axis, Å	60 ± 3	59 ± 1
Polydispersity	0.15 ± 0.10	0.16 ± 0.10		–	–
Volume, Å^3	1.56 × 10^6	1.9 × 10^6		6.3 × 10^6	6.0 × 10^6

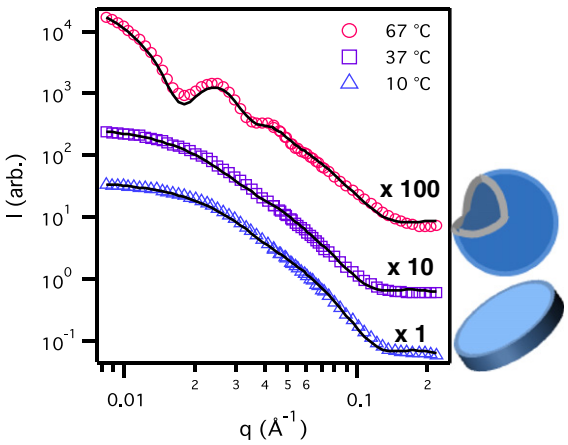

Fig. 9. The SANS data of 10 mg/mL DPPC/DHPC/DPPG/PEG2000-DSPE in PBS buffer at different temperatures following the thermal sequence: from 10 (triangles), 37 (squares) and 67 (circles) °C. The solid curves are the best fits. The SANS data are rescaled by a factor (from 1 to 100) for better visual clarity.

Table 9
Parameters of various models that best fit the SANS data of 10 mg/mL DPPC/DHPC/DPPG/PEG-DSPE in PBS buffer at different temperatures.

T, °C	10	37	67	
Models	PRD		PSSS	
Radius, Å	93.6 ± 2.0	115.7 ± 3.0	Inner radius, Å	149.8 ± 1.0
Thickness, Å	48.5 ± 0.5	49.8 ± 0.7	Thickness, Å	38.9 ± 0.4
Polydispersity	0.17 ± 0.03	0.15 ± 0.05	0.17 ± 0.05	
Volume, Å^3	1.33 × 10^6	2.09 × 10^6	1.4 × 10^7	

leading to a significant variation in the lipid composition of the NPs. Since DHPC adapts to a high-curvature environment, serving as the "edge stabilizer" for nanodiscs, insufficiency of DHPC molecules therefore promotes the self-folding of nanodiscs into ULVs, consistent with our first observation.

The same can be said for the low-T samples in the presence of PBS, since the low-C_{lp} larger discoidal structure has less edge and thus requires less DHPC to be stabilized compared to the high-C_{lp} smaller discoidal structure. At high T, the rate of structural transition (nanodisc-to-vesicle) is also slower if sufficient DHPC associates with the NPs in the case of high-C_{lp} samples. It has also been reported that slower structural transition favors ULV over MLV formation [39]. This explains why the high-C_{lp} ULVs and low-C_{lp} MLVs are found in Fig. 10(b). Finally, more DHPC softens the bilayer, leading to more flexible and homogenously distributed membrane, which prefers to adopt a spherical than an oblate shape to minimize the surface tension. This is also consistent with the observation in Fig. 10(d).

4.3. Effect of PBS

The salt effect on the morphology of bicellar mixtures has been reported elsewhere [37]. The influence mainly comes from the screening of the Coulombic interaction between NPs. In fact, the coalescence process can be described by Smoluchowski population model combined with the DLVO double-layer theory [40]. The current study shows that PBS effectively induces larger discs, ULV and MLV structures [Fig. 4, 10 (b)], possibly because of the fast coalescence consistent with the previous report [39].

4.4. PEG effect

One of the main themes of this report is to understand the PEG effect on the NP structures and thus a better control of the self-assembled nanodiscs is achievable. The result shows that the addition of 5 mol% of PEG2000-DSPE does not affect the formation of nanodiscs. Instead, it further stabilizes the nanodiscs in all the cases studied, consistent with the report in literature [64]. Figs. 1 and 6 provide an insight to the PEG effect on stability of nanodiscs [also in Fig. 10(c)]. The result shows that nanodiscs are stable in the presence of PEG2000-DSPE even at temperatures above the T_M of DPPC, i.e., in the L_α phase. It should be noted that all the samples had been equilibrated at the temperature for more than ½ h before the SANS measurements were taken. Nevertheless, it cannot be proved if the structures obtained from SANS data are thermodynamically stable. Fig. 11 shows the DLS data of the DPPC/DPPG/DHPC and DPPC/DPPG/DHPC/PEG2000-DSPE mixtures in PBS buffer at room temperature. Small NPs (presumably nanodiscs) were initially found in both solutions. After 70 min large particles overwhelmed in the DPPC/DPPG/DHPC mixtures consistent with the TEM micrograph [Fig. 4(b)], while the NPs remain stable for 5 days in the DPPC/DPPG/DHPC/PEG2000-DSPE solution with only small amount of larger aggregates. It should be noted that since the distribution functions obtained in DLS are mass-weighted, the small number of large aggregates in Fig. 11 (b) should not affect the best fitting result of the SANS data.

Another noteworthy effect of PEG2000-DSPE on the spontaneous structures is that it counteracts with the effect of PBS salt. The comparison between Figs. 4 and 8 indicates that the addition of PEG2000-DSPE effectively inhibits the formation of MLVs. As mentioned previously, this

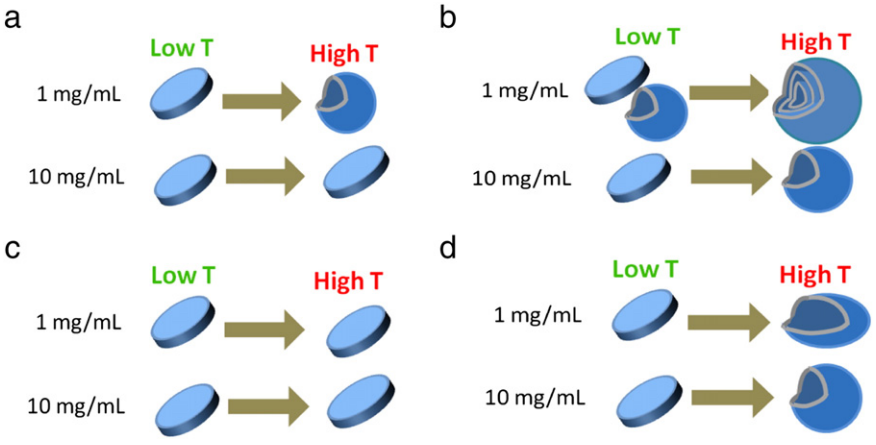

Fig. 10. Temperature-triggered structural transformation in the cases of C_{lp} = 1 mg/mL and 10 mg/mL: (a) in the absence of PBS salt and PEG2000-DSPE, (b) in the presence of PBS salt but in the absence of PEG2000-DSPE, (c) in the absence of PBS salt but in the presence of PEG2000-DSPE and (d) in the presence of PBS salt and PEG2000-DSPE.

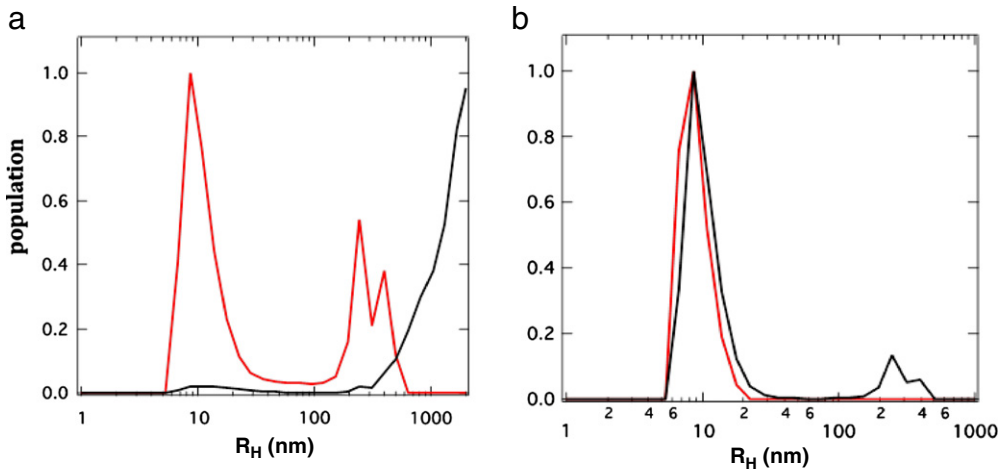

Fig. 11. Particle size distributions measured by DLS: (a) DPPC/DHPC/DPPG and (b) DPPC/DHPC/DPPG/PEG2000-DSPE in PBS solutions as prepared (red) and after a period of time (black): 70 min in (a) and 5 days in (b).

is possibly due to the steric interaction of the PEG chains which slows the coalescence process and self-folding rate of the nanodiscs, leading to a unilamellar structure.

5. Conclusion

Uniform lipid-based nanodiscs can be obtained in a mixture of DPPC/DPPG/DHPC and DPPC/DPPG/DHPC/PEG2000-DSPE through self-assembly and the formation is robust. These nanodiscs can serve as precursors of the uniform ULVs. SANS was applied to probe the morphologies of the NPs in the mixtures as a function of C_{lp}, temperature, in the presence and absence of PBS and PEG2000-DSPE. It is clearly shown that DPPC/DHPC/DPPG nanodiscs and ULVs self-assemble at low and high T (compared to T_M of DPPC), respectively, as previously reported DMPC/DHPC/DMPG system [27]. High-C_{lp} samples allow more DHPC associated with the NPs and consequently stabilize the rim of the nanodiscs. PBS screens the charge interaction between NPs and thus promotes the coalescing rate of the nanodiscs, leading to the formation of polydispersed large discs (or ULVs) and MLVs at low and high temperature, respectively. The DPPC/DHPC/DPPG nanodiscs are reasonably stable in water at low temperature. Although the nanodiscs in the absence of PEG2000-DSPE exhibit low stability in PBS buffer (at physiologically relevant concentration), the PEG2000-DSPE is able to stabilize nanodiscs and inhibit the formation of MLVs. This is possibly attributed to the steric effect caused by the PEG chains, inhibiting or slowing down the kinetics of the coalescence. To the best of our knowledge, this study presents one of the first attempts to understand the effect of PEG2000-DSPE on the self-assembled nanodiscs. This knowledge can provide important insight to the low uptake of surface PEGylated NPs by RES. Future study will focus on investigating the location of the PEG2000-DSPE and understanding the relationship between the disc coalescing rate and spontaneous morphology.

Acknowledgment

M.-P. N., Y. L. and M. L. would like to acknowledge the financial support by NSF-CMMI 1131589 and the neutron scattering facilities at HFIR and SNS of the Oak Ridge National Laboratory as well as Dr. Shuo Qian's and Dr. William Heller's assistance in SANS instrumentation.

Appendix A. Supplementary data

Supplementary data to this article can be found online at http://dx.doi.org/10.1016/j.bbamem.2014.02.004.

References

[1] C.R. Sanders, G.C. Landis, Reconstitution of membrane proteins into lipid-rich bilayered mixed micelles for NMR studies, Biochemistry 34 (1995) 177–182.
[2] C.R. Sanders, R.S. Prosser, Bicelles: a model membrane system for all seasons? Structure 6 (1998) 1227–1234.
[3] C.R. Sanders, K. Oxenoid, Customizing model membranes and samples for NMR spectroscopic studies of complex membrane proteins, Biochim. Biophys. Acta Biomembr. 1508 (2000) 129–145.
[4] G. Zandomeneghi, P.T.F. Williamson, A. Hunkeler, B.H. Meier, Switched-angle spinning applied to bicelles containing phospholipid-associated peptides, J. Biomol. NMR 25 (2003) 125–132.
[5] I. Marcotte, M. Auger, Bicelles as model membranes for solid-and solution-state NMR studies of membrane peptides and proteins, Concepts Magn. Reson. A 24 (2005) 17–35.
[6] A. Diller, C. Loudet, F. Aussenac, G. Raffard, S. Fournier, M. Laguerre, A. Grélard, S.J. Opella, F.M. Marassi, E.J. Dufourc, Bicelles: A natural 'molecular goniometer' for structural, dynamical and topological studies of molecules in membranes, Biochimie 91 (2009) 744–751.
[7] U.H.N. Dürr, M. Gildenberg, A.S. Ramamoorthy, The magic of bicelles lights up membrane protein structure, Chem. Rev. 112 (2012) 6054–6074.
[8] Faham, J.U. Bowie, Bicelle crystallization: a new method for crystallizing membrane proteins yields a monomeric bacteriorhodopsin structure, J. Mol. Biol. 316 (2002) 1–6.
[9] M. Caffrey, Membrane protein crystallization, J. Struct. Biol. 142 (2003) 108–132.
[10] L.C. Johansson, A.B. Wöhri, G. Katona, S. Engström, R. Neutze, Membrane protein crystallization from lipidic phases, Curr. Opin. Struct. Biol. 19 (2009) 372–378.
[11] R. Ujwal, J.U. Bowie, Crystallizing membrane proteins using lipidic bicelles, Methods 55 (2011) 337–341.
[12] A.C. Kimble-Hill, A review of factors affecting the success of membrane protein crystallization using bicelles, Front. Biol. 8 (2013) 261–272.
[13] P.A. Luchette, T.N. Vetman, R.S. Prosser, R.E. Hancock, M.-P. Nieh, C.J. Glinka, S. Krueger, J. Katsaras, Morphology of fast-tumbling bicelles: a small angle neutron scattering and NMR study, Biochim. Biophys. Acta Biomembr. 1513 (2001) 83–94.
[14] I. Marcotte, F. Separovic, M. Auger, S.M. Gagné, A multidimensional ^{1}H NMR investigation of the conformation of methionine–enkephalin in fast-tumbling bicelles, Biophys. J. 86 (2004) 1587–1600.
[15] A. Andersson, L. Mäler, Size and shape of fast-tumbling bicelles as determined by translational diffusion, Langmuir 22 (2006) 2447–2449.
[16] R.S. Prosser, F. Evanics, J.L. Kitevski, M.S. Al-Abdul-Wahid, Current applications of bicelles in NMR studies of membrane-associated amphiphiles and proteins, Biochemistry 45 (2006) 8453–8465.
[17] A. Andersson, H. Biverståhl, J. Nordin, J. Danielsson, E. Lindahl, L. Mäler, The membrane-induced structure of melittin is correlated with the fluidity of the lipids, Biochim. Biophys. Acta Biomembr. 1768 (2007) 115–121.
[18] W. Ye, J. Liebau, L. Mäler, New membrane mimetics with galactolipids: lipid properties in fast-tumbling bicelles, J. Phys. Chem. B 117 (2013) 1044–1050.
[19] E.K. Tiburu, S. Tyukhtenko, H. Zhou, D.R. Janero, J. Struppe, A. Makriyannis, Human cannabinoid 1 GPCR C-terminal domain interacts with bilayer phospholipids to modulate the structure of its membrane environment, AAPS J. 13 (2011) 92–98.
[20] Z. Lu, W.D. Van Horn, J. Chen, S. Mathew, R. Zent, C.R. Sanders, Bicelles at low concentrations, Mol. Pharm. 9 (2012) 752–761.
[21] L. Barbosa-Barros, C. Barba, M. Cócera, L. Coderch, C. López-Iglesias, A. de La Maza, O. López, Effect of bicellar systems on skin properties, Int. J. Pharm. 352 (2008) 263–272.
[22] L. Barbosa-Barros, A. de La Maza, J. Estelrich, A.M. Linares, M. Feliz, P. Walther, R. Pons, O. López, Penetration and growth of DPPC/DHPC bicelles inside the stratum corneum of the skin, Langmuir 24 (2008) 5700–5706.

[23] G. Rodríguez, M. Cócera, L. Rubio, C. Alonso, R. Pons, C. Sandt, P. Dumas, C. López-Iglesias, A. de La Maza, O. López, Bicellar systems to modify the phase behaviour of skin stratum corneum lipids, Phys. Chem. Chem. Phys. 14 (2012) 14523–14533.
[24] L. Barbosa-Barros, G. Rodríguez, C. Barba, M. Cócera, L. Rubio, J. Estelrich, C. López-Iglesias, A. De La Maza, O. López, Bicelles: lipid nanostructured platforms with potential dermal applications, Small 8 (2012) 807–818.
[25] L. van Dam, G. Karlsson, K. Edwards, Direct observation and characterization of DMPC/DHPC aggregates under conditions relevant for biological solution NMR, Biochim. Biophys. Acta Biomembr. 1664 (2004) 241–256.
[26] L. van Dam, G. Karlsson, K. Edwards, Morphology of magnetically aligning DMPC/DHPC aggregates — perforated sheets, not disks, Langmuir 22 (2006) 3280–3285.
[27] M.-P. Nieh, C.J. Glinka, S. Krueger, R.S. Prosser, J. Katsaras, SANS study on the effect of lanthanide ions and charged lipids on the morphology of phospholipid mixtures, Biophys. J. 82 (2002) 2487–2498.
[28] M.-P. Nieh, V.A. Raghunathan, C.J. Glinka, T.A. Harroun, G. Pabst, J. Katsaras, Magnetically alignable phase of phospholipid "bicelle" mixtures is a chiral nematic made up of wormlike micelles, Langmuir (2004) 7893–7897.
[29] R. Soong, M.-P. Nieh, E. Nicholson, J. Katsaras, P.M. MacDonald, Bicellar mixtures containing pluronic F68: morphology and lateral diffusion from combined SANS and PFG NMR studies, Langmuir 26 (2010) 2630–2638.
[30] M.-P. Nieh, V.A. Raghunathan, G. Pabst, T.A. Harroun, K. Nagashima, H. Morales, J. Katsaras, P.M. MacDonald, Temperature driven annealing of perforations in bicellar model membranes, Langmuir (2011) 4838–4847.
[31] G. Raffard, S. Steinbruckner, A. Arnold, J.H. Davis, E.J. Dufourc, Temperature–composition diagram of dimyristoylphosphatidylcholine–dicaproylphosphatidylcholine 'bicelles' self-orienting in the magnetic field: a solid state ^{2}H and ^{31}P NMR study, Langmuir 16 (2000) 7655–7662.
[32] E. Sternin, D. Nizza, K. Gawrisch, Temperature dependence of DMPC/DHPC mixing in a bicellar solution and its structural implications, Langmuir 17 (2001) 2610–2616.
[33] L. Maceachern, A. Sylvester, A. Flynn, A. Rahmani, M.R. Morrow, Dependence of bicellar system phase behavior and dynamics on anionic lipid concentration, Langmuir 29 (2013) 3688–3699.
[34] M.-P. Nieh, T. Harroun, V. Raghunathan, C. Glinka, J. Katsaras, Concentration-independent spontaneously forming biomimetic vesicles, Phys. Rev. Lett. 91 (2003) 158105.
[35] M.-P. Nieh, V. Raghunathan, S.R. Kline, T. Harroun, C.-Y. Huang, J. Pencer, J. Katsaras, Spontaneously formed unilamellar vesicles with path-dependent size distribution, Langmuir 21 (2005) 6656–6661.
[36] M.-P. Nieh, J. Katsaras, X. Qi, Controlled release mechanisms of spontaneously forming unilamellar vesicles, Biochim. Biophys. Acta Biomembr. 1778 (2008) 1467–1471.
[37] S. Mahabir, D. Small, M. Li, W. Wan, N. Kučerka, K. Littrell, J. Katsaras, M.-P. Nieh, Growth kinetics of lipid-based nanodiscs to unilamellar vesicles-A time-resolved small angle neutron scattering (SANS) study, Biochim. Biophys. Acta Biomembr. 1828 (2013) 1025–1035.
[38] J.A. Losonczi, J.H. Prestegard, Improved dilute bicelle solutions for high-resolution NMR of biological macromolecules, J. Biomol. NMR 12 (1998) 447–451.
[39] M.-P. Nieh, P. Dolinar, N. Kučerka, S.R. Kline, L.M. Debeer-Schmitt, K.C. Littrell, J. Katsaras, Formation of kinetically trapped nanoscopic unilamellar vesicles from metastable nanodiscs, Langmuir 27 (2011) 14308–14316.
[40] A. Hu, T.-H. Fan, J. Katsaras, Y. Xia, M. Li, M.-P. Nieh, Lipid-Based Nanodiscs as Models for Studying Mesoscale Coalescence — A Charge Limited Case, Soft Matters (2014) (in press).
[41] J.A. Whiles, K.J. Glover, R.R. Vold, E.A. Komives, Methods for studying transmembrane peptides in bicelles: consequences of hydrophobic mismatch and peptide sequence, J. Magn. Reson. 158 (2002) 149–156.
[42] J. Lind, J. Nordin, L. Mäler, Lipid dynamics in fast-tumbling bicelles with varying bilayer thickness: effect of model transmembrane peptides, Biochim. Biophys. Acta Biomembr. 1778 (2008) 2526–2534.
[43] P.-W. Yang, T.-L. Lin, Y. Hu, U.-S. Jeng, Small-angle x-ray scattering studies on the structure of MixedDPPC/dic 7pc micelles in aqueous solutions, Chin. Phys. 50 (2012) 349–356.
[44] W. Shinoda, R. Devane, M.L. Klein, Zwitterionic lipid assemblies: molecular dynamics studies of monolayers, bilayers, and vesicles using a new coarse grain force field, J. Phys. Chem. B 114 (2010) 6836–6849.
[45] H. Lee, R.W. Pastor, Coarse-grained model for pegylated lipids: effect of pegylation on the size and shape of self-assembled structures, J. Phys. Chem. B 115 (2011) 7830–7837.
[46] S. Wang, R.G. Larson, Coarse-grained molecular dynamics simulation of tethered lipid assemblies, Soft Matter 9 (2013) 480–486.
[47] Y. Jiang, H. Wang, J.T. Kindt, Atomistic simulations of bicelle mixtures, Biophys. J. 98 (2010) 2895–2903.
[48] A.L. Klibanov, K. Maruyama, V.P. Torchilin, L. Huang, Amphipathic polyethyleneglycols effectively prolong the circulation time of liposomes, FEBS Lett. 268 (1990) 235–237.
[49] A. Gabizon, F. Martin, Polyethylene glycol-coated (pegylated) liposomal doxorubicin. Rationale for use in solid tumours, Drugs 54 (1997) 15–21.
[50] S.R. Kline, Reduction and analysis of SANS and USANS data using IGOR Pro, J. Appl. Crystallogr. 39 (2006) 895–900.
[51] L.A. Feigin, D.I. Svergun, Determination of the Integral Parameters of Particles, in: Structure Analysis by Small-Angle X-Ray and Neutron, Plenum Publishing Inc., New York and London, 1987. 60–105.
[52] J.F. Nagle, M.C. Wiener, Structure of fully hydrated bilayer dispersions, Biochim. Biophys. Acta Biomembr. 942 (1988) 1–10.
[53] P.L. Yeagle, The Structure of Biological Membranes, Second ed. CRC Press LLC, Boca Raton, London, New York and Washington, D.C., 2005. (Chapter 2).
[54] M.-P. Nieh, N. Kučerka, J. Katsaras, Spontaneously formed unilamellar vesicles, Methods Enzymol. 465 (2009) 3–20.
[55] N. Kučerka, M.-P. Nieh, J. Katsaras, Fluid phase lipid areas and bilayer thicknesses of commonly used phosphatidylcholines as a function of temperature, Biochim. Biophys. Acta Biomembr. 1808 (2011) 2761–2771.
[56] Y. Sakuma, N. Urakami, T. Taniguchi, M. Imai, Asymmetric distribution of cone-shaped lipids in a highly curved bilayer revealed by a small angle neutron scattering technique, J. Phys. Condens. Matter 23 (2011) 284104.
[57] O. Garbuzenko, Y. Barenholz, A. Priev, Effect of grafted PEG on liposome size and on compressibility and packing of lipid bilayer, Chem. Phys. Lipids 135 (2005) 117–129.
[58] J.B. Hayter, J. Penfold, Determination of micelle structure and charge by neutron small-angle scattering, Colloid Polym. Sci. 261 (1983) 1022–1030.
[59] N.L. Yamada, Kinetic process of formation and reconstruction of small unilamellar vesicles consisting of long- and short-chain lipids, Langmuir 28 (2012) 17381–17388.
[60] P. Lesieur, M.A. Kiselev, L.I. Barsukov, D. Lombardo, Temperature-induced micelle to vesicle transition: kinetic effects in the DMPC/NaC system, J. Appl. Crystallogr. 33 (2000) 623–627.
[61] J. Leng, S.U. Egelhaaf, M.E. Cates, Kinetics of the micelle-to-vesicle transition: aqueous lecithin-bile salt mixtures, Biophys. J. 85 (2003) 1624–1646.
[62] E.J. Dufourc, J.-F. Faucon, G. Fourche, J. Dufourcq, T. Gulik-Krzywicki, M. le Maire, Reversible disc-to-vesicle transition of melittin-DPPC complexes triggered by the phospholipid acyl chain melting, FEBS J. 201 (1986) 205–209.
[63] R.J.M. Tausk, J. Karmiggelt, C. Oudshoorn, J. Overbeek Physical, Chemical studies of short chain lecithin homologues. I. Influence of the chain length of the fatty acid ester and of electrolytes on the critical micelle concentration, Biophys. Chem. 1 (1974) 175–183.
[64] M.M. Zetterberg, K. Reijmar, M. Pränting, A. Engström, D.I. Andersson, K. Edwards, PEG-stabilized lipid disks as carriers for amphiphilic antimicrobial peptides, J. Control. Release 156 (2011) 323–328.